Journal of Energy Chemistry 54 (2021) 620–625

Contents lists available at ScienceDirect

Journal of Energy Chemistry

journal homepage: www.elsevier.com/locate/jechem

http://www.journals.elsevier.com/journal-of-energy-chemistry/

Chlorinated polymer solar cells simultaneously enhanced by fullerene and non-fullerene ternary strategies

Longzhu Liu [a,b,1], Pengjie Chao [b,1], Daize Mo [b], Feng He [b,c,*]

[a] School of Chemistry and Chemical Engineering, Harbin Institute of Technology, Harbin 150001, Heilongjiang, China
[b] Shenzhen Grubbs Institute and Department of Chemistry, Southern University of Science and Technology, Shenzhen 518055, Guangdong, China
[c] Guangdong Provincial Key Laboratory of Catalysis, Southern University of Science and Technology, Shenzhen 518055, Guangdong, China

ARTICLE INFO

Article history:
Received 12 May 2020
Revised 7 June 2020
Accepted 10 June 2020
Available online 25 June 2020

Keywords:
Chlorination
Polymer solar cell
Multi-component
Fullerene
Non-fullerene

ABSTRACT

To achieve efficient polymer solar cells (PSCs) with full utilization of the whole spectrum, the multi-component devices are of great importance to be deeply explored, especially for their capability of one-step fabrication. However, the research about one same binary system simultaneously derivated various multi-component PSC is still very limited. Herein, we achieved the whole constructions from one binary host to different ternary systems and even the quaternary one. The ternary strategies with fullerene acceptor, $PC_{71}BM$, and non-fullerene acceptor, BT_6IC-BO-4Cl, as the third component, both boosted the device efficiencies of PBT4Cl-Bz: IT-4F binary system from about 9% to comparatively beyond 11%. Despite the comparable improvement of performance, there existed other similarities and differences in two ternary strategies. In detail, the isotropic carrier transport of $PC_{71}BM$ which largely elevated the fill factor (FF) in the corresponding devices, while the strong absorption of BT_6IC-BO-4Cl enhanced the short current density (J_{sc}) most. More interestingly, quaternary devices based on PBT4Cl-Bz: IT-4F: $PC_{71}BM$: BT_6IC-BO-4Cl could combine both advantages of fullerene and non-fullerene ternary strategies, further pumped the J_{sc} from 16.44 to the highest level of 19.66 mA cm^{-2} among all devices, eventually resulted in an optimized efficiency of 11.69%. It reveals that both fullerene and non-fullerene ternary strategies have their unique feature to elevate the device performance either by efficient isotropic carrier transport or better coverage of whole sunlight spectrum and easy tunable energy levels from organic materials. The key is how to integrate the two pathways in one system and provide a more competitive solution facing high-quality PSCs.

1. Introduction

Polymer solar cells (PSCs), as an environmentally friendly candidate, has been a hot spot for green energy, because of their huge potential for marketing production [1,2]. Through endeavors for decades, the state-of-art performance of PSCs has broken 15% [3] by innovative materials design [4], and the ternary strategies further pushed the power conversion efficiency (PCE) to another peak of 16% [5,6]. Since the ternary strategies were put forward [7,8], many ternary systems were successfully following in succession because minor third additives can complement the host absorption, adjust the newly-formed energy level, regulate the morphology, and largely enhance the carrier transport [9–11]. According to the property of the third additive, ternary systems could be simply classified into two groups, fullerene and non-fullerene additive ternary systems. Fullerene additives, such as $PC_{61}BM$, $PC_{71}BM$, Bis-$PC_{71}BM$, and ICBA have been widely used to pump solar device performance in the last decade mainly due to their three-dimensional isotropic electron transport feature [11]. For another thing, recent reports also argued that the miscibility of blend components could be improved by forming alloy co-acceptor under strong intermolecular combination between different moieties [12–15]. Besides the miscibility, the spectral complementarity also needs to consider for better sunlight absorbance. However, defects of weak absorption seriously limit the further development of fullerene derivatives as the third component in the device. Therefore, to solve this problem, varieties of non-fullerene additives were developed to collocate the traditional binary system. Rather than relatively fixed and weak absorption in the visible region of

* Corresponding author at: Shenzhen Grubbs Institute and Department of Chemistry, Southern University of Science and Technology, Shenzhen 518055, Guangdong, China.
E-mail address: hef@sustech.edu.cn (F. He).
[1] These authors contributed equally to this work.

https://doi.org/10.1016/j.jechem.2020.06.014

fullerene type additives, their non-fullerene competitors demonstrated more flexibility on structure designs and resulted in the much broader absorption at the visible and even near-infrared regions, and also more versatile to fit the energy levels with other components in ternary devices [16–18].

Herein, to understand the critical roles of the fullerene and non-fullerene additives in device performance blooming, which has rarely discussed and compared together in the same binary system, we successfully fabricated two series of ternary devices based on binary solar cells with chlorinated PBT4Cl-Bz as donor and IT-4F as co-acceptor [19]. Among these devices, one ternary system selected the $PC_{71}BM$ as the third component, which comprehensively improved the photovoltaic performance, especially the fill factor (FF) enhanced from 58.87% to 66.95% because of the increased charge carrier mobility and more efficient extraction in the ternary system. Another non-fullerene ternary system used BT_6IC-BO-4Cl as the additive, benefitting from expanded absorbance spectrum to the near-infrared region, thus the best improvement of the non-fullerene-additive system contributed most to the short current density (J_{sc}), elevating from 16.44 to 18.88 mA cm^{-2} in this non-fullerene ternary device. By both strategies, the device efficiencies over 11% can be achieved from the relatively low efficiency of 9% in their binary system. Finally, supplemental quaternary devices were further explored using both fullerene and non-fullerene as co-acceptor, and the results deduced that their respective merits could integrate into a quaternary system together to boost the photovoltaic performance. From a device engineering perspective, our work reveals the different mechanisms of fullerene and non-fullerene co-acceptor in the ternary system and provides the organic solar cell community a comprehensive pathway to realize the whole spectrum covering and more efficient multi-component devices construction.

2. Experimental

2.1. Materials

PBT4Cl-Bz (M_n = 31000, PDI = 2.1), IT-4F, BT_6IC-BO-4Cl were all synthesized by our laboratory. $PC_{71}BM$ was purchased from the 1-material company.

2.2. PSCs fabrication and characterization

2.2.1. PSCs fabrication

The inverted device structure is ITO/ZnO/ active layer/MoO_3(10-nm)/Ag(100 nm). A clean ITO was prepared. Then ZnO and active layer were spinning coated on it subsequently. The spin speed and time for ZnO was 3000 rpm/25 s. All the active layer solution was dissolved as D/A(total) = 1: 1.5 in chlorobenzene (CB) at 10 mg/mL, 1800 rpm/35 s. After annealed at 100 °C/10 min, MoO_3 and Ag were evaporated at a pressure of 5×10^{-6} Pa through a mask of 0.045 cm^2.

2.2.2. PSCs characterization

Steady-state current–voltage (*J–V*) curves of devices were tested by a Keithley 2400 source-measurement unit under AM 1.5 G spectrum from a solar simulator (Enlitech. Inc) calibrated by a silicon reference cell (Hamamatsu S1133 color, with KG-5 visible fiith) and the relationship of J_{sc} to the light intensity was measured by steady-state current–voltage measurement, the light intensity was modulated by neutral density filters (NDF) with different values of optical density (OD). The external quantum efficiency (EQE) was measured by a solar cell–photodetector responsibility measurement system (Enlitech. Inc). Thin film thickness was obtained by surface profilemeter (Tencor, Alpha-500). The mobility of electron was tested by fitting the current-bias characteristics in dark utilizing a field-independent space charge limited current (SCLC) model according to the Mott-Gurney rule of $J = \frac{9}{8}\varepsilon_0\varepsilon_r\mu\frac{V^2}{L^3}$.The device structures for hole-only and electron-only devices are respectively followed as ITO/PEDOT: PSS/active layer/MoO_3/Ag and ITO/ZnO/active layer/PDINO/Ag. The film morphology was conducted by transmission electron microscope (TEM) JEOL-JEM 2100F microscope and atomic force microscopy (AFM, Veeco Metrology Group/Digital Instruments) with tapping mode.

3. Results and discussion

3.1. Chemical structures and photovoltaic performances

Fig. 1(a–d) shows the chemical structures of selected molecules to construct the ternary systems. PBT4Cl-Bz, IT-4F were respectively served as host donor and host acceptor, which has been reported as binary chlorinated PSCs before [19,20]. BT_6IC-BO-4Cl will be reported later. $PC_{71}BM$ was introduced as a guest to construct the fullerene-additive ternary system while the BT_6IC-BO-4Cl comprised of the non-fullerene-additive ternary one. From Table 1, it can be easily observed that two ternary strategies can efficiently enhance the PCE of PBT4Cl-Bz: IT-4F binary device from 9.08% to almost 11.30%, increasing by almost 25% at most. The difference is that the $PC_{71}BM$-based ternary device slightly elevated the open-circuit voltage (V_{oc}) of the binary system from 0.94 to 0.96 V, while the BT_6IC-BO-4Cl-based ternary device slightly decreased to 0.92 V in the opposite direction. This can be explained by the energy levels of the third co-acceptor involved. As shown in Fig. 1(e), $PC_{71}BM$ has a much higher LUMO level while BT_6IC-BO-4Cl has a shallower LUMO, which is in turn influencing the V_{oc} in the blend ternary devices [20,21]. As for the elevated J_{sc} and FF, J_{sc} considerably increased from 16.44 to 17.79 mA cm^{-2} after 20% $PC_{71}BM$ addition, and even surged to 18.88 mA cm^{-2} due to the high tolerance of ratio of BT_6IC-BO-4Cl addition (50%). In contrast, FF of $PC_{71}BM$-based ternary devices (from 58.87% to 66.95%) only took a tiny advantage than that (from 58.87% to 65.29%) of BT_6-IC-BO-4Cl-based ternary devices. In general, the fullerene ternary strategy roundly improved the photovoltaic performance parameters, especially the FF, thus a champion PCE of 11.38% was achieved. Compared with the fullerene ternary system, BT_6IC-BO-4Cl additive devoted most to the J_{sc} which was adequate to offset a slight decrease of V_{oc} and a slightly inferior FF, leading to a comparable PCE of 11.32%. These differences are more vividly annotated in their *J-V* curves in Fig. 2. And photovoltaic performances of both ternary devices with different deviations around the best ratio are supported in Tables S1, S2, and Fig. S1.

3.2. Optical properties and morphology control

To better understand the increasing of current density in two ternary systems, normalized absorption spectra of pristine films of each component and their blend films were plotted in Fig. 3(a, b). Locations of maximum absorption peak and absorption onset were summarized in Tables S3 and S4. A stronger or broad absorption of the active layer is much helpful to improve the J_{sc} of the binary system [22,23]. Reflecting by the external quantum efficiency (EQE) curves in Fig. 3(c), the fullerene-additive ternary system took on an upward trend of light response, covering such a wide wavelength region from 400 to 800 nm; while another BT_6IC-BO-4Cl ternary system mainly extended the light response from 780 to 900 nm, eventually making this non-fullerene ternary device a very broad light response covering from 300 to 900 nm. As shown in Fig. 3(d), ΔEQE curves (calculated by $EQE_{ternary}(\lambda) - EQE_{binary}(\lambda)$) could more clearly amplify the light-response capability of these

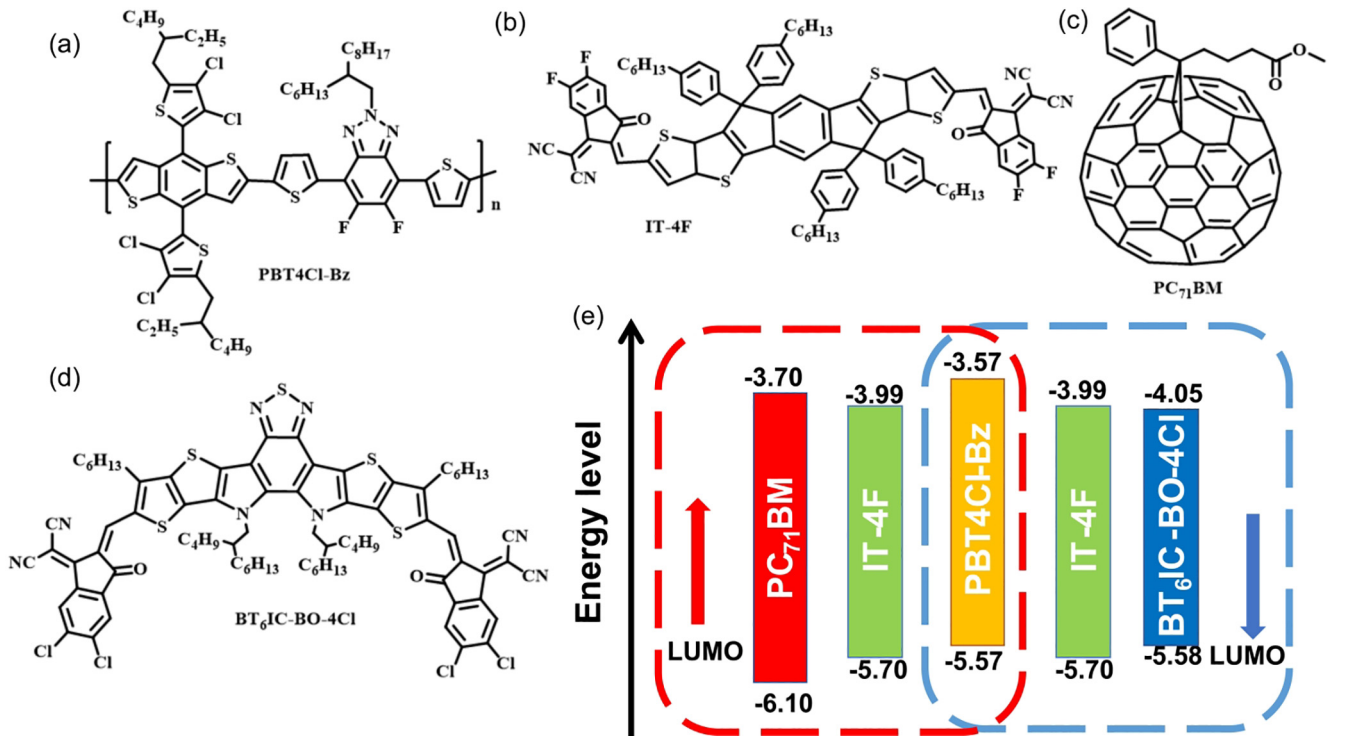

Fig. 1. Chemical structures of molecules (a) PBT4Cl-Bz; (b) IT-4F; (c) $PC_{71}BM$; (d) BT_6IC-BO-4Cl; and (e) energy levels between $PC_{71}BM$ and PBT4Cl-Bz: IT-4F; and between BT_6IC-BO-4Cl and PBT4Cl-Bz: IT-4F ternary systems.

Table 1
Photovoltaic performance parameters of fullerene-additive ternary devices, binary devices, and non-fullerene-additive ternary devices under 100 mW cm^{-2} AM 1.5 G irradiation.

Composition	V_{oc} (V)	J_{sc} (mA cm^{-2})	FF (%)	PCE (%)	J_{cal}[b] (mA cm^{-2})
PBT4Cl-Bz:IT-4F	0.94	16.44	58.87	9.08 (8.73 ± 0.35)[a]	15.96
PBT4Cl-Bz:IT-4F:PC71BM	0.96	17.79	66.95	11.38 (11.13 ± 0.25)	17.29
PBT4Cl-Bz:IT-4F:BT_6IC-BO-4Cl	0.92	18.88	65.29	11.32 (11.03 ± 0.29)	18.31

[a] Average value ± standard deviation was obtained from 16 independent devices.
[b] The calculated J_{sc} values from EQE curves.

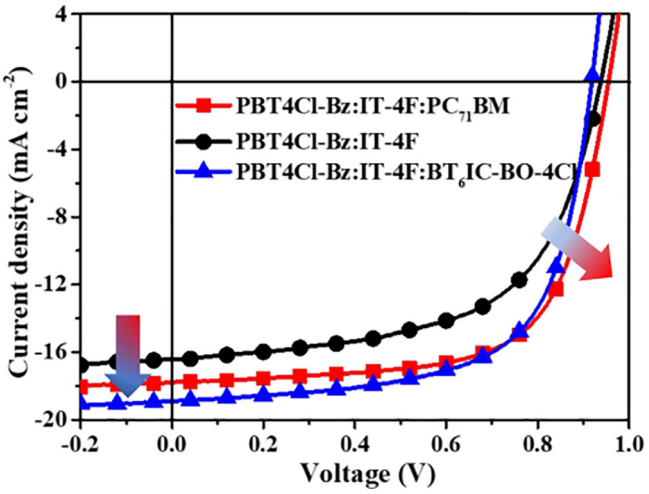

Fig. 2. *J-V* curves of fullerene-additive ternary devices, binary devices, and non-fullerene-additive ternary devices under 100 mW cm^{-2} AM 1.5 G irradiation.

two ternary systems, which also correspond well to the absorption spectra and the trend developed of EQE curves. Significantly, about 50% contribution of ΔEQE was derived from the absorption of non-fullerene additive BT_6IC-BO-4Cl, which in agreement well with the surge of J_{sc} as discussed above. However, J_{sc} and FF are not completely decided by the light-to-photon capability, but also influenced by the film morphology [24,25]. Characterized from the atomic force microscopy (AFM) (Fig. S2(a–c)) results, the root-mean-square (RMS) roughness of parent binary blend film was about 1.22 nm, and smaller RMS roughness (about 1.00 nm) of ternary blends suggested that both ternary blends had more smooth surfaces, indicating that the film morphology could be further optimized by the third addition either of $PC_{71}BM$ or BT_6IC-BO-4Cl. These blend films had been further measured by transmission electron microscopy (TEM) (Fig. S2(d–f)), the binary blend showed some big aggregations as shown in Fig. S2(d). The $PC_{71}BM$-additive ternary preserved most of the features from the binary microstructure but indicated a much smaller and suitable phase separation, no big aggregations could be found in this case. Yet the BT_6IC-BO-4Cl-additive ternary blend showed obvious differences from its binary film, in which there was more compact and well-arranged morphology observed. As a result, both ternary blends could obtain much better interpenetrate morphologies compared with their binary system, thus facilitating the carrier transport, and then finally enhancing the J_{sc} and FF.

3.3. Carrier transport study

To verify the carrier transport process, thereby gaining a deeper insight into the mechanisms of different ternary solar cells, we

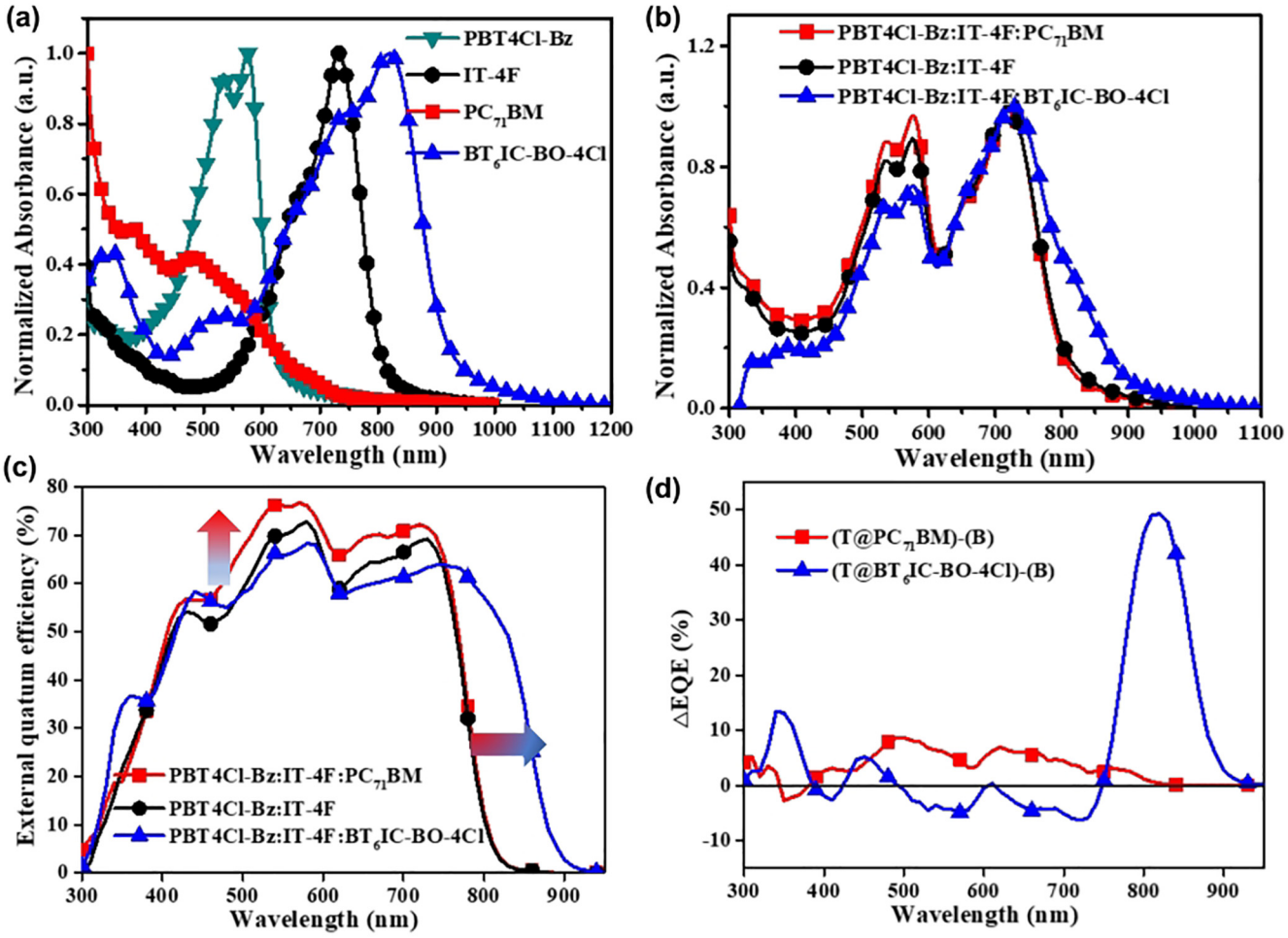

Fig. 3. (a) Normalized absorption of neat films and (b) blend film of PBT4Cl-Bz: IT-4F, PBT4Cl-Bz:IT-4F: $PC_{71}BM$, PBT4Cl-Bz:IT-4F: BT_6IC-BO-4Cl. (c) EQE curves of binary and two ternary systems. (d) ΔEQE between ternary systems with different additive and binary systems.

tested the maximum exciton generation rate (G_{max}) and exciton dissociation probabilities (η_{diss}, defined as J_{ph}/J_{sat}) by J_{ph} *vs.* V_{eff} curves in Fig. 4(a). When applied effective reverse bias, it is assumed that all photogenerated excitons split into free carriers at the saturation platform, so the G_{max} defines as J_{sat}/qL was only determined by the quantities of harvesting photons [26,27]. However, the binary device was hard to quickly saturate like two ternary devices, which only got a η_{diss} of 0.85, agreeing with its low J_{sc} and FF. Although the fullerene and non-fullerene ternary devices showed similar η_{diss} of 0.96 and 0.95, their values of G_{max} were 1.04×10^{28} m^{-3} S^{-1} for BT_6IC-BO-4Cl ternary device, which was much higher than that of $PC_{71}BM$-based ternary device (0.957×10^{28} m^{-3} S^{-1}). The competitive exciton dissociation but higher exciton generation of BT_6IC-BO-4Cl-based ternary device also consistent with the higher J_{sc} in both ternary systems.

To efficiently transport the separated excitons, the carrier mobility is important as well. The space charge limited current (SCLC) method was applied to measure the electron-only (μ_e) and hole-only (μ_h) devices of binary and two kinds of ternary devices in dark. According to Fig. S3 and Table S5, dual ternary devices gained higher mobility nevertheless electron mobility or hole mobility than that of binary devices ($\mu_e = 6.2 \times 10^{-4}$ cm^2 V^{-1} S^{-1}, $\mu_h = 4.4 \times 10^{-4}$ cm^2 V^{-1} S^{-1}). Moreover, $PC_{71}BM$-based devices largely strengthen electron mobility (μ_e = 8.7×10^{-4} cm^2 V^{-1} S^{-1}) than BT_6IC-BO-4Cl-based devices (μ_e = 7.5×10^{-4} cm^2 V^{-1} S^{-1}). Whereas balanced coefficient (counted by μ_e/μ_h or μ_h/μ_e) of binary device deviated to 1.41, the coefficient of two ternary devices almost approached 1.25 comparably. Thereby, more efficient and balanced carrier mobility was greatly useful to elevate the J_{sc} and FF of ternary ones. In parallel, the whole process accompanied with unavoidable carrier recombination. Fig. 4(b) described the fitting curves about $J_{sc} \propto I^S$, in which S nearly approached 1, the bimolecular recombination could be insignificant [28,29]. Binary devices suffered more bimolecular recombination than its two ternary devices because the lowest fit slope equaled to 0.88 for the binary system, but the ternary devices exhibited commensurate suppressed recombination with a fit slope of about 0.94.

For FF is the result of the competition between the charge recombination and charge extraction [30,31]. Then transient photovoltage (TPV) technique [32] and transient photocurrent (TPC) technique [33] were applied to detect among the three devices under steady state in Fig. 4(c, d). Binary device lagged behind two ternary systems nevertheless of the carrier lifetime (t_τ, 1.49 μs) or the carrier extraction (t_s, 0.97 μs). However, when the recombination and extraction achieved a delicate balance, it could result in a comparative PCE like both ternary devices present here. The $PC_{71}BM$-based ternary device owned more prior carrier extraction speed (t_s = 0.35 μs) yet a shorter carrier lifetime (t_τ = 3.12 μs) than that of BT_6IC-BO-4Cl-based devices (t_s = 0.41 μs, t_τ = 3.26 μs). More efficient exciton extraction of $PC_{71}BM$-based ternary device meant higher collective efficiency of carrier-to-electrodes [32]. And a longer lifetime would enable a smaller recombination cur-

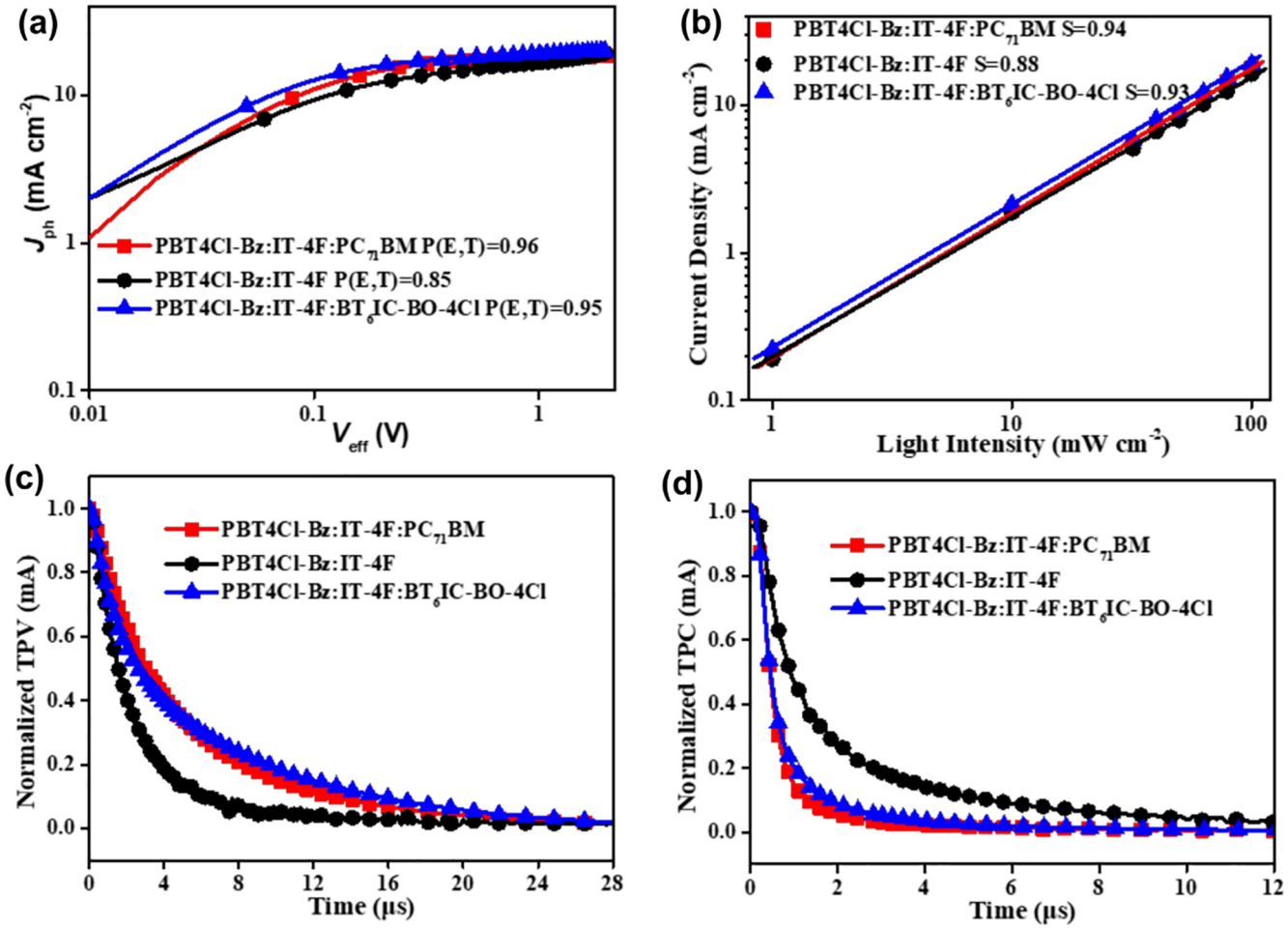

Fig. 4. (a) J_{ph} *vs.* V_{eff} curves; (b) current density dependence of light intensity curves; (c) normalized TPV curves and (d) TPC curves of binary and ternary devices.

rent [33], so BT_6IC-BO-4Cl-based devices allowed less trap for carrier quench. Simultaneously, comparable extraction also avoids the heavy carrier accumulation thus giving a good explanation of the photovoltaic performances of the BT_6IC-BO-4Cl ternary devices and PC_{71}BM ternary devices.

3.4. Quaternary devices combined with fullerene and non-fullerene ternary strategies

Naturally, to fully make use of their respective fortes, we tried to fabricate the quaternary devices based on PBT4Cl-Bz:IT-4F: PC_{71}BM: BT_6IC-BO-4Cl at their best ratio (1: 1: 0.2: 0.5, Table S6). This quaternary combination surprisingly reached even higher J_{sc} of 19.66 mA cm^{-2}, and a V_{oc} of 0.92 V, an FF of 64.40 thus leading to the highest level of PCE (11.69%). Corresponding *J-V* curve and EQE spectrum were also well in agreement in Fig. S4. More interestingly, concerned about ΔEQE curve of $EQE_{quaternary}(\lambda) - EQE_{ternary}(\lambda)$ in Fig. S5, and contrasted with Fig. 3(d), the positive value distribution just respectively attributed to the fullerene and non-fullerene positive part, which supported us a bold inspiration that more quaternary devices could combine more advantageous and functionalized components [34–37]. In Table S7, we summarized groups of ternary systems that derivated by as similar as possible binary system, and grouped them as either activated by fullerene guest or non-fullerene guest from recent reports to support potential quaternary choices [38–40]. Also, from such a database, it could be seen that one same binary system that simultaneously derivated fullerene and non-fullerene ternary strategies were rarely discussed. So, it also highlights the urgency to explore the results present here, which provides a better understanding of the critical roles in each added acceptor in multi-component devices.

4. Conclusions

In conclusion, adopting different ternary strategies either based on fullerene additive or non-fullerene additive has been an effective method to boost the photovoltaic performances of the binary device. The best PCE based on PBT4Cl-Bz: IT-4F was respectively perked from 9.08% up to 11.38% in PC_{71}BM-involved ternary device and up to 11.32% in BT_6IC-BO-4C-involved ternary device. Contrasted with the binary device, the most distinguished enhancement in PC_{71}BM-additive devices was the FF, increasing from 58.87% to 66.95%, while BT_6IC-BO-4Cl-based ternary devices were more inclined to elevating the J_{sc}, from 16.44 to 18.88 mA cm^{-2}. It was suggested that whether in PC_{71}BM-based ternary devices or BT_6IC-BO-4Cl-based ternary devices, phase morphology was delicately regulated, and carrier transport was strengthened, leading to an improvement of J_{sc} and FF. Besides comparable exciton dissociation and restrained recombination in two ternary systems, the isotropic electron transport and carrier extraction enabled the notable rise of FF based on the PC_{71}BM guest, whereas the extended light absorption spectrum, more efficient exciton generation and inhibited recombination current allowed the superiority of J_{sc} of BT_6IC-BO-4Cl-based ternary device. Worth mentioning, the upward and broader trend in light response could well be embod-

ied in PBT4Cl-Bz: IT-4F: $PC_{71}BM$: BT_6IC-BO-4Cl quaternary devices, which pushed the J_{sc} to a peak value of 19.66 mA cm^{-2}, and then obtained a champion efficiency of 11.69%, increasing by nearly 29% compared with the binary one. The multi-component PSCs from binary to fullerene/non-fullerene ternary and even their compatible quaternary strategies are expected to offer more helpful insights and guidance for more efficient organic photovoltaic applications.

Declaration of Competing Interest

The authors declare that they have no known competing financial interests or personal relationships that could have appeared to influence the work reported in this paper.

Acknowledgements

The authors thank the financial support by the National Natural Science Foundation of China (21733005, 21975115, 51773087), Shenzhen Fundamental Research Program (KQJSCX20180319114442157, JCYJ20170817111214740, JCYJ20180302180238419) and Shenzhen Nobel Prize Scientists Laboratory Project (C17213101), Guangdong Provincial Key Laboratory of Catalysis (No. 2020B121201002), Guangdong Innovative and Entrepreneurial Research Team Program (2016ZT06G587) and Shenzhen Sci-Tech Fund (KYTDPT20181011104007). We thank the SUSTech Core Research Facilities for the AFM and TEM measurements, and the supported by Center for Computational Science and Engineering at SUSTech.

Appendix A. Supplementary data

Supplementary data to this article can be found online at https://doi.org/10.1016/j.jechem.2020.06.014.

References

[1] D. Corzo, K. Almasabi, E. Bihar, S. Macphee, D. Rosas-Villalva, N. Gasparini, S. Inal, D. Baran, Adv. Mater. Technol. 4 (2019) 1900040.
[2] H.J. Lai, Q.Q. Zhao, Z.Y. Chen, H. Chen, P.J. Chao, Y.L. Zhu, Y.W. Lang, N. Zhen, D. Z. Mo, Y.Z. Zhang, F. He, Joule 4 (2020) 688–700.
[3] J. Yuan, Y. Zhang, L. Zhou, G. Zhang, H.-L. Yip, T.-K. Lau, X. Lu, C. Zhu, H. Peng, P. A. Johnson, M. Leclerc, Y. Cao, J. Ulanski, Y. Li, Y. Zou, Joule 3 (2019) 1140–1151.
[4] W. Li, L. Ye, S. Li, H. Yao, H. Ade, J. Hou, Adv. Mater. 30 (2018) e1707170.
[5] Q. An, X. Ma, J. Gao, F. Zhang, Sci. Bull. 64 (2019) 504–506.
[6] B. Fan, D. Zhang, M. Li, W. Zhong, Zh. Zeng, L. Ying, F. Huang, Y. Cao, Sci. China Chem. 62 (2019) 746–752.
[7] L. Lu, T. Xu, W. Chen, E.S. Landry, L. Yu, Nat. Photon. 8 (2014) 716–722.
[8] L. Lu, W. Chen, T. Xu, L. Yu, Nat. Commun. 6 (2015) 7327.
[9] N. Gasparini, A. Salleo, I. McCulloch, D. Baran, Nat. Rev. Mater. 4 (2019) 229–242.
[10] W. Xu F. Gao, Mater. Horiz. 5 (2018) 206-221.
[11] S. Li, W. Liu, C.Z. Li, M. Shi, H. Chen, Small 13 (2017) 1701120.
[12] Y. Zhu, A. Gadisa, Z. Peng, M. Ghasemi, L. Ye, Z. Xu, S. Zhao, H. Ade, Adv. Energy Mater. 9 (2019) 1900376.
[13] Q. Zhao, Z. Xiao, J. Qu, L. Liu, H. Richter, W. Chen, L. Han, M. Wang, J. Zheng, Z. Xie, L. Ding, F. He, ACS Energy Lett. 4 (2019) 1106–1114.
[14] M. Nam, M. Cha, H.H. Lee, K. Hur, K.T. Lee, J. Yoo, I.K. Han, S.J. Kwon, D.H. Ko, Nat. Commun. 8 (2017) 14068.
[15] H.B. Naveed, W. Ma, Joule 2 (2018) 621–641.
[16] A. Zeng, M. Pan, B. Lin, T.-K. Lau, M. Qin, K. Li, W. Ma, X. Lu, C. Zhan, H. Yan, Solar RRL 4 (2019) 1900353.
[17] Z. Zhou, S. Xu, J. Song, Y. Jin, Q. Yue, Y. Qian, F. Liu, F. Zhang, X. Zhu, Nat. Energy 3 (2018) 952–959.
[18] R. Yu, S. Zhang, H. Yao, B. Guo, S. Li, H. Zhang, M. Zhang, J. Hou, Adv. Mater. 29 (2017) 1700437.
[19] P. Chao, L. Liu, J. Zhou, J. Qu, D. Mo, H. Meng, Z. Xie, F. He, Y. Ma, ACS Appl Energy Mater. 1 (2018) 6549–6559.
[20] P. Chao, N. Johner, X. Zhong, H. Meng, F. He, J. Energy Chem. 39 (2019) 208–216.
[21] K. Li, Y. Wu, Y. Tang, M.A. Pan, W. Ma, H. Fu, C. Zhan, J. Yao, Adv. Energy Mater. 9 (2019) 1901728.
[22] T. Liu, Z. Luo, Y. Chen, T. Yang, Y. Xiao, G. Zhang, R. Ma, X. Lu, C. Zhan, M. Zhang, C. Yang, Y. Li, J. Yao, H. Yan, Energy Environ. Sci. 12 (2019) 2529–2536.
[23] T. Liu, Q. Zhao, H. Wang, J. Qu, P. Chao, N. Zheng, H. Lai, D. Mo, F. He, Mater. Chem. Front. 3 (2019) 1859–1865.
[24] R.S. Gurney, W. Li, Y. Yan, D. Liu, A.J. Pearson, T. Wang, J. Energy Chem. 37 (2019) 148–156.
[25] G. Zhou, H. Ding, L. Zhu, C. Qiu, M. Zhang, T. Hao, W. Feng, Y. Zhang, H. Zhu, F. Liu, J. Energy Chem. 47 (2020) 180–187.
[26] X. Song, N. Gasparini, M.M. Nahid, S.H.K. Paleti, J.-L. Wang, H. Ade, D. Baran, Joule 3 (2019) 846–857.
[27] L. Zhong, L. Gao, H. Bin, Q. Hu, Z.-G. Zhang, F. Liu, T.P. Russell, Z. Zhang, Y. Li, Adv. Energy Mater. 7 (2017) 1602215.
[28] Q. Chang, H. Chen, J. Yuan, Y. Hu, J. Hai, W. Liu, F. Cai, J. Hong, X. Xiao, Y. Zou, J. Energy Chem. 51 (2020) 7–13.
[29] L.J.A. Koster, V.D. Mihailetchi, H. Xie, P.W.M. Blom, Appl. Phys. Lett. 87 (2005) 203502.
[30] D. Bartesaghi, J. Kniepert, S. Roland, M. Turbiez, D. Neher, L.J.A. Koster, Nat. Commun. 6 (2015) 7083.
[31] N. Gasparini, X. Jiao, T. Heumueller, D. Baran, G.J. Matt, S. Fladischer, E. Spiecker, H. Ade, C.J. Brabec, T. Ameri, Nat. Energy 1 (2016) 118.
[32] C.G. Shuttle, B. O'Regan, A.M. Ballantyne, J. Nelson, D.D.C. Bradley, J. de Mello, J. R. Durrant, Appl. Phys. Lett. 92 (2008) 093311.
[33] C.G. Shuttle, A. Maurano, R. Hamilton, B. O'Regan, J.C. de Mello, J.R. Durrant, Appl. Phys. Lett. 93 (2008) 183501.
[34] D. Yan, J. Xin, W. Li, S. Liu, H. Wu, W. Ma, J. Yao, C. Zhan, A.C.S. Appl, Mater. Interfaces 11 (2019) 766–773.
[35] Z. Bi, Q. Zhu, X. Xu, H.B. Naveed, X. Sui, J. Xin, L. Zhang, T. Li, K. Zhou, X. Liu, X. Zhan, W. Ma, Adv. Funct. Mater. 29 (2019) 1806804.
[36] L. Yang, L. Yan, W. You, J. Phys. Chem. Lett. 4 (2013) 1802–1810.
[37] L. Liu, H. Chen, W. Chen, F. He, J. Mater. Chem. A 7 (2019) 7815–7822.
[38] B. Wang, Y. Fu, Q. Yang, J. Wu, H. Liu, H. Tang, Z. Xie, J. Mater. Chem. C 7 (2019) 10498–10506.
[39] M. Zhang, Z. Xiao, W. Gao, Q. Liu, K. Jin, W. Wang, Y. Mi, Q. An, X. Ma, X. Liu, C. Yang, L. Ding, F. Zhang, Adv. Energy Mater. 8 (2018) 1801968.
[40] X. Du, J. Zhao, H. Zhang, X. Lu, L. Zhou, Z. Chen, H. Lin, C. Zheng, S. Tao, J. Mater. Chem. A 7 (2019) 20139–20150.